

# Individual Content and Motion Dynamics Preserved Pruning for Video Diffusion Models

Yiming Wu<sup>1\*</sup> Huan Wang<sup>2\*</sup> Zhenghao Chen<sup>3\*</sup> Dong Xu<sup>1†</sup>

<sup>1</sup>School of Computing and Data Science, The University of Hong Kong

<sup>2</sup>School of Engineering, Westlake University

<sup>3</sup>School of Information and Physical Sciences, The University of Newcastle, Australia

{yimingwu, dongxu}@hku.hk    zhenghao.chen@newcastle.edu.au    wanghuan@westlake.edu.cn

## Abstract

*The high computational cost and slow inference time are major obstacles to deploying the video diffusion model (VDM) in practical applications. To overcome this, we introduce a new Video Diffusion Model Compression approach using individual content and motion dynamics preserved pruning and consistency loss. First, we empirically observe that deeper VDM layers are crucial for maintaining the quality of **motion dynamics** e.g., coherence of the entire video, while shallower layers are more focused on **individual content** e.g., individual frames. Therefore, we prune redundant blocks from the shallower layers while preserving more of the deeper layers, resulting in a lightweight VDM variant called VDMini. Additionally, we propose an **Individual Content and Motion Dynamics (ICMD) Consistency Loss** to gain comparable generation performance as larger VDM, i.e., the teacher to VDMini i.e., the student. Particularly, we first use the **Individual Content Distillation (ICD) Loss** to ensure consistency in the features of each generated frame between the teacher and student models. Next, we introduce a **Multi-frame Content Adversarial (MCA) Loss** to enhance the motion dynamics across the generated video as a whole. This method significantly accelerates inference time while maintaining high-quality video generation. Extensive experiments demonstrate the effectiveness of our VDMini on two important video generation tasks, **Text-to-Video (T2V)** and **Image-to-Video (I2V)**, where we respectively achieve an average  $2.5 \times$  and  $1.4 \times$  speed up for the I2V method SF-V and the T2V method T2V-Turbo-v2, while maintaining the quality of the generated videos on two benchmarks, i.e., UCF101 and VBench.*

## 1. Introduction

Video generation has achieved significant progress in the recent few years, owing to the rapid development of the video

diffusion model (VDM) [3, 50, 52]. Despite the promising advances in video diffusion quality, the high computational costs and slow inference time hinder the democratization of video generation tasks in real-world applications. For instance, generating a two-second video by Stable Video Diffusion [3] costs more than 25 seconds on an A100 GPU, and generating a 5 seconds video costs more than 5 minutes on online platforms such as KLing [1] and DreamMachine [32].

To address the computational challenges in VDM, two primary strategies can be adopted: reducing the number of sampling steps and decreasing model parameters. Recent research has predominantly focused on minimizing sampling steps. For instance, some works have extended consistency distillation techniques [52, 54, 59], while other approaches have employed adversarial training methods [38, 61] to VDM. On the other hand, model compression techniques for VDM remain under-explored. While the common model compression techniques such as pruning [15, 20, 24, 33, 45, 55] and knowledge distillation [5, 21] have shown promising results on image diffusion models [7, 29, 35], directly applying these methods to VDM is still challenging.

First, unlike the image diffusion models, where block importance can be relatively easily estimated by assessing the quality of a single generated image, pruning in VDMs requires a more complex evaluation. In VDMs, it's essential to assess both the quality of content in individual frames and the motion dynamic consistency across the entire generated video [13]. Through comprehensive analysis, we have observed that the deeper layers of VDMs are crucial for maintaining multi-frame content consistency, particularly in terms of motion dynamics across frames. In contrast, the shallower layers primarily contribute to the generation of individual RGB content in each frame. This insight allows us to selectively prune shallower layers while preserving the deeper ones, which optimizes computational efficiency without compromising video quality. With such observation, we present a light-weight VDM architecture **VDMini**, which

\*The first three authors have equal contributions.

†Corresponding Author.

achieves a  $2.5\times$  and  $1.4\times$  speedup for the image-to-video (I2V) and the text-to-video (T2V) generation tasks.

In order to further improve the performance of pruned VDM (*i.e.* VDMini), we perform a fine-tuning procedure to achieve comparable generation quality as the unpruned VDM. Due to the aforementioned challenges, here we concentrate on both individual content (*i.e.*, spatial smoothness of a single frame) and motion dynamics (coherence of an entire video) quality consistency. Therefore, we introduce a new Individual Content and Motion Dynamics (ICMD) Consistency loss to maintain the consistency between pruned VDMini (*i.e.*, student) and unpruned VDM (*i.e.*, teacher). Inspired by the previous work on image generation [29], we leverage knowledge distillation to maintain individual content consistency. Since applying an additional knowledge distillation loss for multi-frame content consistency would be redundant, we introduce an adversarial loss on the video-level feature to reinforce the overall content consistency.

We validate the effectiveness of our approach on two representative video generation tasks: Image-to-Video (I2V) and Text-to-Video (T2V). Combining the aforementioned block pruning technique and the ICMD loss. We achieve a  $2.5\times$  speedup on the I2V model SF-V [61] and a  $1.4\times$  speedup on the T2V model T2V-Turbo-V2 [34], while maintaining comparable generation quality on both UCF101 and VBench benchmarks. Our contributions are summarized as follows:

- We conduct a comprehensive assessment for the importance estimation of VDM blocks based on individual content and motion dynamics, followed by pruning the redundant layers to achieve model compression. To this end, we present a lightweight VDM variant VDMini, which achieves a significant speedup in inference time.
- To ensure quality consistency between the pruned VDMini and the unpruned VDM, we introduce the ICMD loss, it consists of two components: the ICD Loss for individual content consistency, which aligns the generated content in each single frame, and the MCA Loss for multi-frame content consistency, which preserves motion dynamics across the entire video. By maintaining frame-level and video-wide consistency, we can align VDMini closely with the unpruned VDM.
- We validate the effectiveness of our approach on two video generation tasks, namely I2V and T2V. Our method achieves a  $2.5\times$  speedup over the I2V model SF-V and a  $1.4\times$  speedup over the T2V model T2V-Turbo-v2 while maintaining comparable quality metrics on standard benchmarks UCF101 and VBench.

## 2. Related Work

### 2.1. Video Generation

Video generation has seen wide exploration in recent years. Traditionally, generative adversarial networks (GANs) [18]

and VAEs [30] have been utilized for this purpose, but they are generally limited to producing low-quality and short-duration videos. The advent of diffusion models and large-scale video datasets has significantly enhanced video generation quality. Initial explorations [28, 60] leverage pre-trained image models for video generation without the need for fine-tuning *i.e.* training-free methods. However, despite the reduction in training requirements, these approaches are limited in terms of both inference speed and generation quality due to their reliance on DDIM Inversion [49].

With the emergence of large-scale video datasets such as WebVid-10M [2] and Panda70M [10], training-based methods have demonstrated significant improvements in generation quality and condition consistency capabilities. Jonathan *et al.* [23] were the first to extend diffusion models to 3D space-time modeling by incorporating factorized space-time attention blocks into a U-Net architecture.

To leverage pre-trained image diffusion models, approaches such as Video LDM [4], Animatediff [19], VideoCrafter2 [9], and Stable Video Diffusion [3] have been developed. These methods introduce temporal layers following the residual and attention blocks of image generation models, and then employ multi-stage fine-tuning on high-quality video datasets, leading to substantial improvements in generation quality.

On the other hand, pure transformer-based models, such as DiT [44] originally used for image generation, have also been extended to video generation. Sora [43] demonstrated impressive results by scaling up transformer-based architectures for video generation. To democratize access to advanced video generation models, Open-Sora [63] and Open-Sora-Plan [31] have been developed to provide open-source options for the community. Moreover, recent work on CogVideoX [58] introduces an Expert Transformer model for long-duration video generation, surpassing previous state-of-the-art models in video generation tasks.

Our approach aims to accelerate the video generation process by compressing existing high-cost models while preserving generation quality. In this work, we focus on two specific video generation tasks: image-to-video (I2V) and text-to-video (T2V), and propose a lightweight model, VDMini, to achieve this goal.

### 2.2. Pruning for Diffusion Models

The excessive size of diffusion models has prompted research on compressing diffusion models via two classic model compression techniques: network pruning, and distillation. Here we summarize the recent advances on them.

SnapFusion [35] is one of the pioneering works that accelerate diffusion models from two aspects: changing the model architecture by pruning [15, 20, 33, 55]; reducing the inference steps by distillation [21, 39, 46]. The central problem of pruning is to measure the relative weight importance.

SnapFusion introduces an importance score comprising two terms: CLIP score drop and latency reduction. They adopt a widely-used “trial-and-error” paradigm [40, 41] to obtain the importance score for each weight module - remove a module of the model and record the CLIP score drop and latency reduction; the modules with the *least* CLIP score drop and *most* latency reduction are considered insignificant and thus removed. After pruning, a new more efficient UNet architecture is delivered, which runs over  $7\times$  faster than its SD-v1.5 counterpart. To reduce the inference steps, SnapFusion introduces a CFG-aware distillation loss that aligns the student model’s output with its teacher’s after applying CFG. Overall, they achieve an unprecedented mobile inference speed of less than 2 seconds on an iPhone 14 Pro and no CLIP score and FID degradation.

Concurrent to SnapFusion, BK-SDM [29] also attempts to accelerate SD models by pruning weight blocks. Unlike SnapFusion, their block importance analysis only considers CLIP score drop and they do not reduce the inference steps. Importantly, they propose a feature-distillation-based retraining strategy to regain model performance after pruning. Overall, BK-SDM achieves 30% to 50% reduction in model size and latency against the original SD model, with a small degradation in CLIP score and FID. The compact BK-SDM-Tiny model is further enhanced to EdgeFusion [6] by leveraging a strong teacher, LCM [37] to reduce inference steps, and high-quality AI-generated data.

MobileDiffusion [62] is a subsequent work that accelerates SD models by improving its architecture and reducing inference steps, too. Like SnapFusion and BK-SDM, it also utilizes pruning to remove redundant residual blocks. Differently, MobileDiffusion proposes even more fine-grained architecture optimizations, such as using more transformers in the middle of U-Net and fewer channels, decoupling self-attention from cross-attention, sharing key-value projections, using separable convolutions, and so on. For reducing inference steps, they adopt the distillation loss from prior works, SnapFusion [35] and UFOGen [57]. Overall, by integrating these optimization techniques, they achieve a remarkable inference speed of 0.2 second on an iPhone 15 Pro.

In addition to the above works that aim to accelerate the SD models, some papers study the pruning methods on relatively small diffusion models. Diff-Pruning [16] prunes the channels of diffusion models by employing the dependency graph tool developed in DepGraph [15] to address the structural dependency problem when pruning models with residual connections. The method is shown effective on small-scale datasets with max image resolution of  $256\times 256$ , no SD models evaluated.

Our paper differs from the works above in that we focus on accelerating a practical *video* diffusion model, while the works above mainly focus on *image* diffusion models.

## 3. Methodology

### 3.1. Preliminaries

**Diffusion Models.** a Diffusion model (DM) consists of two major processes: 1. a forward diffusion process that adds noise to the input data iteratively and 2. a reverse denoising process that removes the predicted noise to recover the original input. In the continuous-time framework [26, 51], let  $p(\mathbf{x}; \sigma)$  as the distribution obtained by adding i.i.d Gaussian noise  $\sigma$  to the data distribution  $p_{data}(\mathbf{x}_0)$ . With a large  $\sigma_{max}$ , the distribution  $p(\mathbf{x}; \sigma_{max})$  is close to the pure noise distribution. Then, the probability flow ordinary differential equation (PF-ODE) is defined as:

$$d\mathbf{x} = -\dot{\sigma}_t \sigma_t \nabla_{\mathbf{x}} \log p(\mathbf{x}, \sigma_t) dt, \quad (1)$$

where the score function  $\nabla_{\mathbf{x}} \log p(\mathbf{x}, \sigma_t)$  is generally approximated by  $\frac{(D_{\theta}(\mathbf{x}; \sigma_t) - \mathbf{x})}{\sigma_t^2}$ . In the EDM framework [26, 27],  $D_{\theta}(\mathbf{x}_t, \sigma_t)$  is parameterized as:

$$D_{\theta} = c_{skip}(t)\mathbf{x}_t + c_{out}(t)f_{\theta}(c_{in}(t)\mathbf{x}_t, c_{noise}(t)), \quad (2)$$

where  $f_{\theta}$  is the learnable neural network trained by minimizing  $L^2$  denoising error, and  $c_{skip}$ ,  $c_{in}$ ,  $c_{out}$ , and  $c_{noise}$  are the time-dependent conditioning coefficients. The I2V models SF-V [61] and SVD [3] are developed based on the EDM framework.

**Consistency Models.** Consistency models (CM) [50, 52] offers a new family of generative models which enforces the learned neural network  $f_{\theta}(\mathbf{x}_t, t)$  maps the arbitrary noise input  $\mathbf{x}_t$  to the clean data  $\mathbf{x}_0$ , and the CM follows the self-consistency property  $f_{\theta}(\mathbf{x}_t, t) = f_{\theta}(\mathbf{x}'_t, t')$ , where  $\mathbf{x}'_t$  and  $\mathbf{x}_t$  represent the samples on the ODE trajectory at different times  $t$  and  $t'$ . Following the preconditioned EDM framework, the CM sets the boundary condition as  $c_{skip}(0) = 1$  and  $c_{out}(0) = 0$ .

One way to train the CM is to use consistency distillation, which distills the pre-trained DMs by minimizing the consistency loss:

$$\mathcal{L}_{CD}(\theta, \theta^-; \Psi) = \mathbb{E} \left[ d \left( f_{\theta}(\mathbf{x}_{t_{n+k}}, t_{n+k}), f_{\theta^-}(\hat{\mathbf{x}}_{t_n}^{\Psi, \omega}, t_n) \right) \right], \quad (3)$$

where  $d$  is the distance function,  $\hat{\mathbf{x}}_{t_n}^{\Psi, \omega}$  is the reversed data by ODE solver  $\Psi$  with classifier-free guidance (CFG) [22] weight  $\omega$ ,  $n$  is the time step for pretrained DM, and  $k$  is step interval. The T2V model T2V-Turbo-v2 [50] is developed based on the CM.

### 3.2. Network Pruning

**Individual Content and Motion Dynamics Preserved Pruning.** Since the different network blocks play distinct roles in generating videos, we should assess the importance

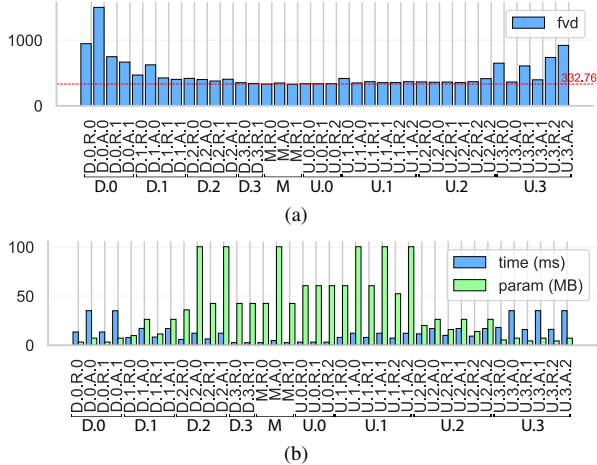


Figure 1. (a) FVD score by removing or replacing the blocks in the U-Net. (**Note that a high FVD score means the block is more important.**) (b) Time and Parameters of the blocks in the U-Net.

of blocks in both *individual content quality* and *motion dynamics*, followed by using the FVD score to quantify the block importance of the SF-V model. Most I2V and T2V models share nearly identical architectures in their diffusion model backbone (*i.e.*, U-Net). For instance, classical VDMs such as VideoCrafter [8] and Open-Sora [63] utilize the exact same U-Net architecture for both I2V and T2V tasks. Consequently, it is reasonable to assume that specific blocks within these U-Nets perform similar roles across both tasks.

By deconstructing the U-Net architecture, we assess the importance of each block by systematically replacing it with either an identity mapping or a single convolutional layer in cases where there is a channel mismatch. This approach allows us to isolate and evaluate the contribution of individual blocks. As illustrated in Fig. 1, “D”, “M”, and “U” denote the DownBlock, MidBlock, and UpBlock, respectively. For a specific block “D.0.R.1”, “R” and “A” represent ResBlock and AttentionBlock, respectively. The first number “0” and the second number “1” represent the block index and the layer index within the block, respectively. Our overall evaluation indicates that removing low-resolution layers in the U-Net significantly raises the FVD score, suggesting a substantial impact on the generation quality of individual frames. In contrast, removing high-resolution layers has a comparatively smaller effect on the FVD score, indicating that these layers are less critical to maintaining the generation quality of each individual frame. Except for the individual generation results, we also examine the visualization results of the pruned U-Net, we empirically find removing the blocks in the “D.2” and “U.1” has a major impact on the motion dynamics of the generated video.

In the end, we prune the second R-A pairs in the DownBlocks and UpBlocks except for the second last DownBlock

“D.2” and the second UpBlock “U.1”, and further remove the MidBlock. The detailed network architecture is provided in the supplement.

Model	Resolution	CLIP Encoder	VAE Encoder	U-Net	VAE Decoder
SF-V	224 × 224	224 × 224	576 × 1024	14 × 72 × 128	14 × 72 × 128
	#Param (M)	632.08	34.16	1524.62	63.58
	Latency (ms)	35	75	512	2832
VDMini-I2V	224 × 224	224 × 224	576 × 1024	14 × 72 × 128	14 × 72 × 128
	#Param (M)	632.08	34.16	<b>940.9</b>	<b>39.17</b>
	Latency (ms)	35	75	<b>345</b>	<b>840.5</b>

Table 1. Comparison of the model architecture and inference latency between SF-V and our proposed VDMini-I2V.

Model	Text Encoder		U-Net	VAE Decoder
	Resolution	77 Tokens	16 × 40 × 64	16 × 40 × 64
T2V-Turbo-v2	Inference Steps	1	16	1
	#Param (M)	354.03	1413.65	49.49
	Latency (ms)	13.57	2554.05	367.66
VDMini-T2V	Inference Steps	1	16	1
	#Param (M)	354.03	<b>817.02</b>	49.49
	Latency (ms)	13.57	<b>1662.26</b>	367.66

Table 2. Comparison of the model architecture and inference latency between T2V-Turbo-v2 and our proposed VDMini-T2V.

**Compressed Network Architecture.** In addition to the U-Net, we find that the VAE decoder used in SF-V significantly contributes to the inference time during the latent decoding process. To address this, we apply both layer pruning and channel pruning to the VAE decoder. Utilizing the introduced network pruning techniques, we develop lightweight VDMini models for I2V and T2V tasks, referred to as VDMini-I2V and VDMini-T2V. As reported in Tab. 1 and Tab. 2, the models demonstrate a 2.5× speedup for I2V tasks and a 1.4× speedup for T2V tasks.

### 3.3. ICMD Consistency Loss

We aim to further enhance the generation performance of the pruned VDMini network by mimicking the intermediate outputs of the U-Net from the original VDM. As previously mentioned, in order to maintain the generation quality of individual frames and the motion dynamics across the video, we propose the Individual Content and Motion Dynamic (ICMD) Consistency Loss. This optimization strategy consists of two parts: Individual Content Distillation (ICD) Loss and Multi-frame Content Adversarial (MCA) Loss.

**Individual Content Distillation Loss:** As illustrated in Fig. 2, ICD loss aims to achieve feature distillation [29] for each individual frame, which transfers the knowledge from the UNet of VDM (*i.e.*, teacher model) to VDMini (*i.e.*, student model). Formally, given a noisy video latent  $\mathbf{x}_t \in \mathbb{R}^{F \times C \times H \times W}$ , the student model  $f^{student}$  is trained by minimizing the distance of intermediate representations between the teacher model  $f^{teacher}$  and the student model:

$$\mathcal{L}_{ICD} = \mathbb{E} \left[ \sum_{l=1}^L d(f_l^{student}(\mathbf{x}_t, t), f_l^{teacher}(\mathbf{x}_t, t)) \right], \quad (4)$$

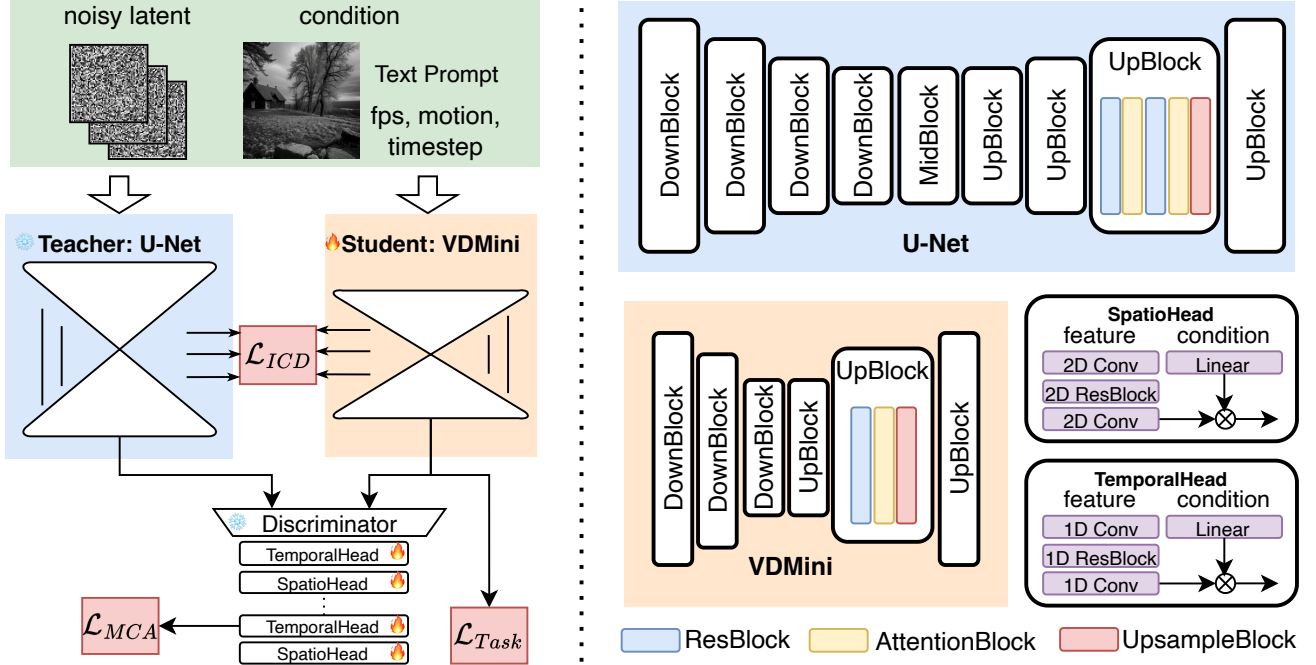


Figure 2. The proposed VDMMini framework for Video Diffusion Model Compression. Left: The retraining process with the proposed ICMD loss, where  $\mathcal{L}_{ICD}$  is the knowledge distillation loss for individual content consistency, and  $\mathcal{L}_{MCA}$  is the adversarial loss for multi-frame content consistency.  $\mathcal{L}_{Task}$  is the task-specific loss function adopted in the base model. Right: The teacher model is pruned by blocks to obtain the student model (*i.e.* VDMMini). The second Block (ResBlock, AttentionBlock) in the DownBlock and UpBlock are removed (Except for the second last DownBlock and UpBlock), and the innermost Blocks (MidBlock, DownBlock, and UpBlock) are entirely removed.

where  $L$  is the number of intermediate representations,  $t$  is the timestep, and  $f_l^{student}(\cdot)$  and  $f_l^{teacher}(\cdot)$  denote the feature representations at the  $l$ -th block of the student and teacher models, respectively.

**Multi-frame Content Adversarial Loss:** With the ICD loss, the student model is forced to mimic the teacher model at the individual content level. However, the motion dynamics across the generated video can not be guaranteed. To address this issue, we introduce the MCA loss to adopt adversarial optimization strategy for preserving the motion dynamics across the generated video. Here, we let the discriminator  $D_\phi$  to distinguish the video latent generated by the student model  $f^{student}$  from the output of the teacher model  $f^{teacher}$  as in Diffusion-GAN [56]. The discriminator  $D_\phi$  comprises a combination of SpatioHead and TemporalHead components with standard 1D and 2D convolutional operations as shown in Fig. 2.

The optimization process can be formulated as:

$$\begin{aligned} \mathcal{L}_{MCA}^{gen} &= -\mathbb{E} [\log (D_\phi (f^{student}(\mathbf{x}_t, t), \sigma_{t'}))], \\ \mathcal{L}_{MCA}^{disc} &= \mathbb{E} [\max(0, 1 + D_\phi (f^{student}(\mathbf{x}_t, t), \sigma_{t'}))] \\ &\quad + \mathbb{E} [\max(0, 1 - D_\phi (f^{teacher}(\mathbf{x}_t, t), \sigma_{t'}))], \end{aligned} \quad (5)$$

where  $\sigma_{t'}$  is the instance noise injected into the samples at

timestep  $t'$ , we follow SF-V to set the noise distribution as a discretized lognormal distribution, and  $t' \in [1, 999]$ .

Along with our newly-proposed ICMD loss, task-specific losses  $\mathcal{L}_{Task}$  are also incorporated during the fine-tuning process. Specifically, for the I2V task, SF-V employs a combination of reconstruction loss and adversarial loss. For the T2V task, T2V-Turbo-v2 utilizes a consistency loss along with a mixture of reward optimization objectives. The final optimization objective is formulated as:

$$\mathcal{L} = \mathcal{L}_{Task} + \lambda_{ICD} \mathcal{L}_{ICD} + \lambda_{MCA} (\mathcal{L}_{MCA}^{gen} + \mathcal{L}_{MCA}^{disc}), \quad (6)$$

where  $\lambda_{ICD}$  and  $\lambda_{MCA}$  are the hyper-parameters to respectively balance the ICD and MCA loss. The optimization details about task-specific losses for the I2V and T2V tasks are provided in the supplementary materials.

## 4. Experiments

### 4.1. Datasets and Evaluation Metrics

**Datasets:** We utilize three datasets for training: OpenVid-1M [42], VidGen-1M [53], and WebVid-10M [2]. OpenVid-1M and VidGen-1M are large-scale video datasets featuring high-quality videos and expressive captions, each containing

over 1 million video-caption pairs. WebVid-10M is a widely-used video dataset collected from the web, encompassing diverse video content. For the I2V task, we first re-implement SF-V using the OpenVid-1M dataset, and then fine-tune the pruned VDMini-I2V model. For the T2V task, we follow the T2V-Turbo-v2 [34] setup, training the model on a mixed dataset of VidGen-1M and WebVid-10M, comprising 180K video-text pairs.

**Evaluation Metrics:** We adopt the same evaluation metrics used in SF-V and T2V-Turbo-v2 for a fair comparison. Specifically, we use the FVD score [17] to measure the quality of the generated videos in the I2V task, which calculates the Fréchet Video Distance between the generated videos and the ground-truth videos from UCF101. Following SF-V, we use the first frame of the video as the conditional input to VDMini to generate the video with a resolution of  $768 \times 1024$ , then resize the video to  $240 \times 320$  for evaluation. The videos are saved as 95% quality JPEG images, following the same setting in [48]. For the T2V task, we assess the performance of our model on VBench [25], which automatically evaluates T2V models in terms of video quality and video prompt consistency, with a total of 16 diverse evaluation dimensions. We set the inference step to 16 for the T2V task, generating videos with a resolution of  $320 \times 512$  and a video length of 16.

## 4.2. Implementation Details

In the experiments, we use 8 NVIDIA A100 GPUs for training the VDMini models and evaluate the models on a single A100 GPU. For training the VDMini-I2V model, we set the resolution of the input video to  $448 \times 576$ . The model is trained with a batch size of 32 (with gradient accumulation of 4) for 10K steps, and the MCA loss is enabled after 3K steps. The learning rate for the U-Net and the discriminator is set to  $1e-4$  and  $1e-5$ , respectively. The VAE decoder is trained with a batch size of 8 for 15K steps. The frame length is sampled from 14 to 25, and the learning rate is initially set to  $5e-5$  and decayed using a cosine annealing schedule. The loss weights for reconstruction loss, perceptual loss, and adversarial loss are set to 1, 1, and 0.2, respectively. For training the VDMini-T2V model, the resolution of the input video is set to  $320 \times 512$ . We set the batch size for fine-tuning to 2 with 8K steps of gradient updating, and the learning rate for the discriminator is set to  $1e-5$ . All other hyper-parameters are kept the same as in the T2V-Turbo-v2 training. The loss weights for ICD loss and MCA loss are set to 0.1 and 1, respectively.

## 4.3. Quantitative Results

**Comparison with Other I2V Methods.** As reported in Tab. 3, VDMini-I2V compresses the U-Net by approximately 40% in terms of parameters and achieves an FVD score of 198.13 after retraining, with no significant drop

Methods	Inference Steps	FVD ↓	Model Size ↓	Latency (ms) ↓
SVD [3]	25	163.43	1.5B	20126
SVD [3]	16	183.98	1.5B	12880
AnimatelCM [54]	8	320.71	1.5B	7346
SF-V [61]	1	166.26	1.5B	512
VDMini-I2V	1	198.13	940M	345

Table 3. Comparison with the existing methods. VDMini-I2V achieves a comparable FVD score with SF-V and 16-step SVD.

Methods	FVD ↓	Latency (ms)
GN Pruning (L2)	288.79	433
GN Pruning (Taylor)	292.18	425
Magnitude Pruning (L2)	271.55	412
Magnitude Pruning (Taylor)	354.51	430
VDMini-I2V	198.13	345

Table 4. Comparison with other baseline pruning approaches. GN Pruning is proposed in DepGraph [15], while Magnitude Pruning aims to remove the smallest magnitude weights in the network. L2 and Taylor are the criteria for importance estimation.

compared to the teacher model (*i.e.* SF-V). When compared to SVD with 16 steps, VDMini-I2V achieves a similar FVD score but is much faster, with a  $37\times$  speedup. This substantial speedup is due to the pruning and fine-tuning strategy employed by VDMini, which reduces the computational complexity of the model without compromising the quality of the generated videos. The reduction in parameters not only accelerates inference time but also decreases the memory footprint, making VDMini-I2V more suitable for deployment in resource-constrained environments. Additionally, the retraining process ensures that the pruned model regains high fidelity in video generation, maintaining the visual quality and temporal coherence of the output videos. This balance between efficiency and performance highlights the practical advantages of VDMini-I2V over the existing state-of-the-art methods.

**Comparison with Other Baseline Pruning Method.** To further validate the effectiveness of the proposed VDMini method, we compare its performance with other structural pruning methods, including Magnitude-based pruning [33] and DepGraph [15]. Magnitude-based pruning focuses on removing the smallest magnitude weights in the network, while DepGraph constructs a dependency graph for the network and iteratively prunes model weights with low-importance scores, using the L2 Norm and first-order Taylor expansion of loss as the importance score. As shown in Tab. 4, our block pruning approach achieves faster latency than these methods for the same model size, primarily because most inference time is spent on high-resolution layers, such as the first DownBlock and the last UpBlock. Since the importance scores used by these pruning methods are not directly correlated with the evaluation protocol, the pruned network architecture may be suboptimal. With the same retraining



Figure 3. Qualitative Results of VDMini-I2V. VDMini-I2V can generate comparable videos with the teacher model SF-V.

process, VDMini-I2V achieves a better FVD score compared to these pruning methods.

$\mathcal{L}_{ICD}$	$\mathcal{L}_{MCA}$	FVD ↓	$\lambda_{ICD}$	$\lambda_{MCA}$	FVD ↓
×	×	299.44	1	1	254.30
✓	×	224.24	0.01	1	286.42
×	✓	257.99	0.1	0.5	198.63
✓	✓	198.13	0.1	1	198.13

Table 5. Effectiveness of loss components.

Table 6. Sensitivity analysis of the hyperparameters.

**Effectiveness of the ICMD Loss.** We conduct ablation studies to validate the effectiveness of the ICMD loss used during the fine-tuning stage. As shown in Tab. 5, enabling  $\mathcal{L}_{ICD}$  and  $\mathcal{L}_{MCA}$  individually results in FVD scores of 224.24 and 257.99, respectively. When both  $\mathcal{L}_{ICD}$  and  $\mathcal{L}_{MCA}$  are combined, the FVD score improves significantly to 198.13. These results highlight the substantial contribution of the ICMD loss to the overall performance of the model.

Methods	Quality Score↑	Semantic Score↑	Total Score↑	Latency (ms)↓
Kling [1]	83.39	75.68	81.85	-
VideoCrafter2 [9]	82.20	73.42	80.44	-
T2V-Turbo-v2 [34]	85.13	77.12	83.52	2554.05
VDMini-T2V	83.33	77.38	82.14	1662.26

Table 7. Comparison of VDMini-T2V with other methods on VBench in terms of Quality Score, Semantic Score, Total Score, and Latency.

**Effectiveness of Loss Weight.** To balance the ICMD loss with the task-specific loss during the training stage, we perform experiments with different hyper-parameters  $\lambda_{ICD}$  and  $\lambda_{MCA}$ . As shown in Tab. 6, we find that the result is sensitive to  $\lambda_{ICD}$ , while more robust to  $\lambda_{MCA}$ . The best result is obtained when  $\lambda_{ICD}$  and  $\lambda_{MCA}$  are set to 0.1 and 1, respectively. This indicates that careful tuning of these

VAE Decoder	PSNR ↑	SSIM ↑	LPIPS ↓
Original	32.30	0.94	0.031
Compressed	31.41	0.93	0.039

Table 8. Quantitative comparison of the image quality metrics on the UCF101 dataset between the original VAE decoder and the compressed VAE decoder.

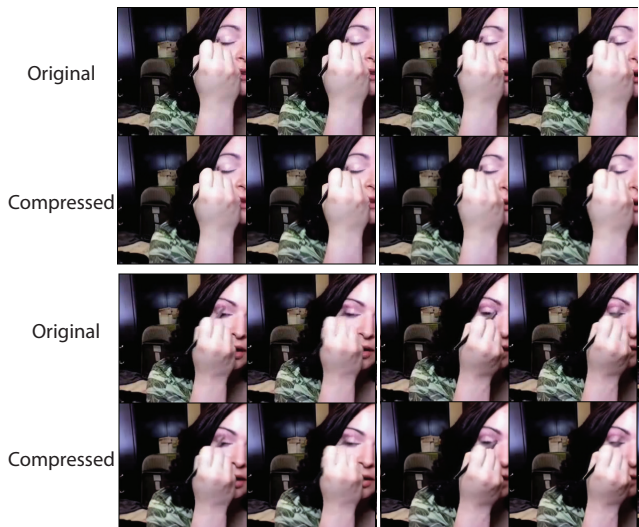


Figure 4. Reconstruction results of the VAE decoder. The image quality metrics of the compressed VAE decoder are close to those of the original VAE decoder.

hyper-parameters is crucial for optimizing the performance of the model.

**Comparison with Other T2V models.** On the other hand, we apply the proposed pruning and fine-tuning strategy on T2V-Turbo-v2, resulting in VDMini-T2V. As shown in Tab. 7, we find that VDMini-T2V reduces 35% inference

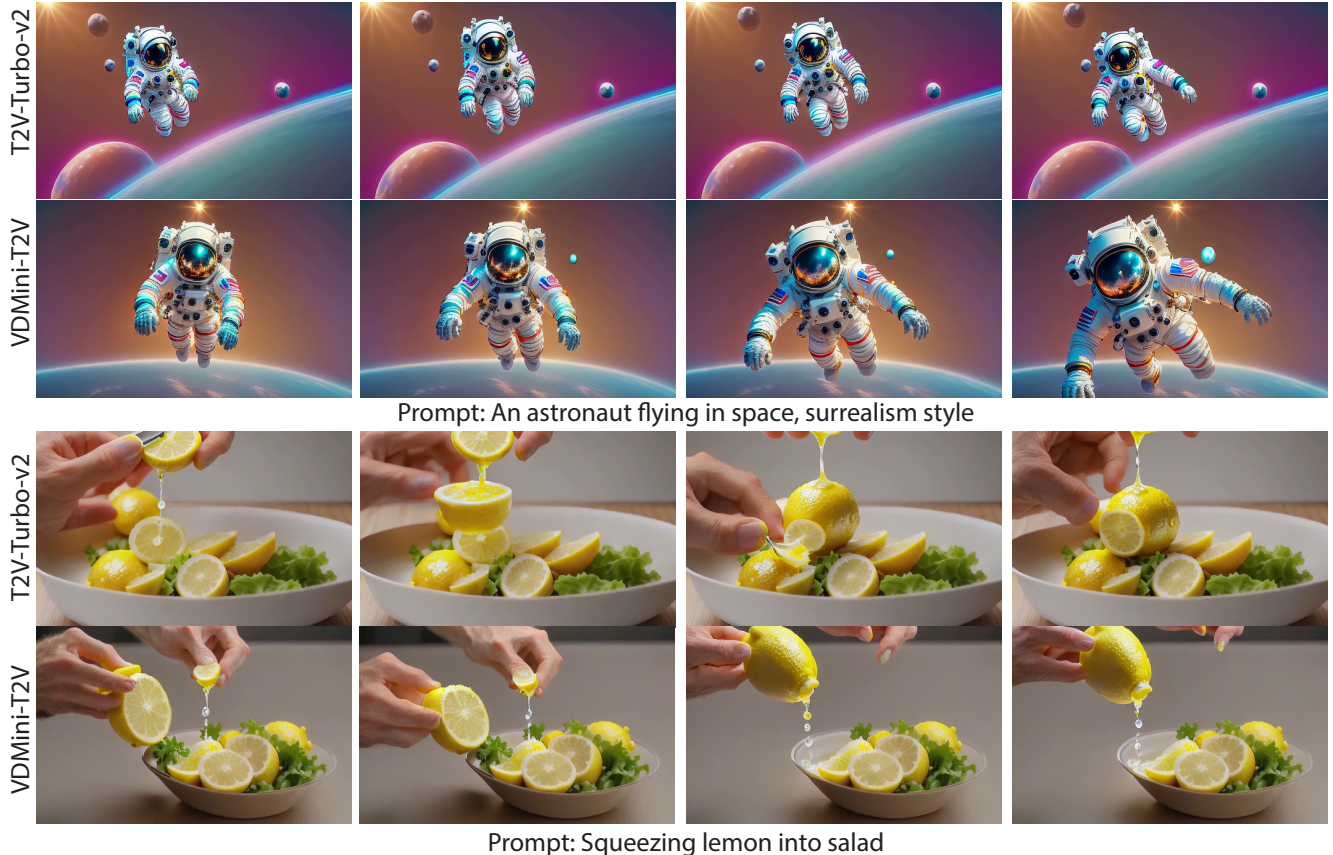


Figure 5. Qualitative Results of VDMini-T2V. VDMini-T2V can generate comparable videos with the teacher model T2V-Turbo-v2.

time compared to T2V-Turbo-v2, with a small degradation on Quality Score after retraining. However, the VDMini-T2V still achieves better results compared to the other models like VideoCrafter2 and KLing.

#### 4.4. Qualitative Results

**Visual Results on the I2V Task.** As shown in Fig. 3, the generated results of our method and other related approaches in the I2V task demonstrate satisfactory performance. The visual results indicate that our method effectively maintains both individual and multi-frame content consistency across frames, preserving similar styles and motions as the teacher model SF-V. In contrast, other methods suffer from blurring or distortion due to motion. Our method exhibits high visual quality and smooth motion with just one step.

#### Reconstruction Results of the Compressed VAE Decoder.

The VAE decoder in the I2V task consumes a significant amount of inference time. To address this, we further compress the VAE decoder in the VDMini-I2V model. We employ layer pruning and channel pruning techniques to accelerate the VAE decoder, followed by fine-tuning on the OpenVid-1M dataset using reconstruction loss, perceptual

loss, and adversarial loss as described in [14]. As shown in Tab. 1, the inference time of the compressed VAE decoder is reduced by 70%, and the model has 30% fewer parameters compared to the original. As provided in Tab. 8, we report the PSNR, SSIM, and LPIPS on the UCF101 dataset, and the reconstruction results are illustrated in Fig. 4.

**Visual Results of VDMini-T2V.** We also present the visual results of the VDMini-T2V model in Fig. 5. The generated videos demonstrate that the VDMini-T2V model is capable of producing high-quality videos that accurately reflect a wide range of input text prompts. The visual consistency and fidelity of the generated videos highlight the effectiveness of our proposed method, ensuring that the VDMini-T2V model maintains the integrity and coherence of the video content while significantly reducing inference time.

## 5. Conclusion

In this work, we have presented VDMini, a lightweight Video Diffusion Models (VDMs). Our approach concentrates on reducing the inference time while maintaining the individual content and multi-frame content quality. The pruning strategy is designed by analyzing the importance of the blocks



in the U-Net as well as the visual quality of the generated video, leading to the removal of redundant shallower layers and preserving the deeper layers to keep the quality of multi-frame content. To further enhance the motion dynamics and quality of the generated video, we apply a multi-frame content adversarial loss with individual content distillation loss during the fine-tuning process. Our experiments demonstrate that VDMini achieves a  $2.5\times$  speedup for Image-to-Video (I2V) methods and a  $1.4\times$  speedup for Text-to-Video (T2V) methods.

**Limitations and Future Work.** Our method is developed for UNet-based VDMs, such as SVD and T2V-Turbo-v2, which may not be optimal for DiT-based VDMs. Besides, the token pruning [11, 12] could be leveraged to accelerate VDMs further. Our future work will focus on accelerating DiT-based VDMs.

## References

- [1] Kling AI. Kling ai. <https://klingai.com/>, 2023. 1, 7
- [2] Max Bain, Arsha Nagrani, Gül Varol, and Andrew Zisserman. Frozen in time: A joint video and image encoder for end-to-end retrieval. In *CVPR*, pages 1728–1738, 2021. 2, 5
- [3] Andreas Blattmann, Tim Dockhorn, Sumith Kulal, Daniel Mendelevitch, Maciej Kilian, Dominik Lorenz, Yam Levi, Zion English, Vikram Voleti, Adam Letts, et al. Stable video diffusion: Scaling latent video diffusion models to large datasets. *arXiv preprint arXiv:2311.15127*, 2023. 1, 2, 3, 6, 12
- [4] Andreas Blattmann, Robin Rombach, Huan Ling, Tim Dockhorn, Seung Wook Kim, Sanja Fidler, and Karsten Kreis. Align your latents: High-resolution video synthesis with latent diffusion models. In *CVPR*, pages 22563–22575, 2023. 2
- [5] Cristian Buciluă, Rich Caruana, and Alexandru Niculescu-Mizil. Model compression. In *SIGKDD*, 2006. 1
- [6] Thibault Castells, Hyoung-Kyu Song, Tairen Piao, Shinkook Choi, Bo-Kyeong Kim, Hanyoung Yim, Changgwun Lee, Jae Gon Kim, and Tae-Ho Kim. Edgefusion: On-device text-to-image generation. *arXiv preprint arXiv:2404.11925*, 2024. 3
- [7] Thibault Castells, Hyoung-Kyu Song, Tairen Piao, Shinkook Choi, Bo-Kyeong Kim, Hanyoung Yim, Changgwun Lee, Jae Gon Kim, and Tae-Ho Kim. Edgefusion: On-device text-to-image generation. *arXiv preprint arXiv:2404.11925*, 2024. 1
- [8] Haoxin Chen, Menghan Xia, Yingqing He, Yong Zhang, Xiaodong Cun, Shaoshu Yang, Jinbo Xing, Yaofang Liu, Qifeng Chen, Xintao Wang, et al. Videocrafter1: Open diffusion models for high-quality video generation. *arXiv preprint arXiv:2310.19512*, 2023. 4
- [9] Haoxin Chen, Yong Zhang, Xiaodong Cun, Menghan Xia, Xintao Wang, Chao Weng, and Ying Shan. Videocrafter2: Overcoming data limitations for high-quality video diffusion models. In *CVPR*, pages 7310–7320, 2024. 2, 7, 13
- [10] Tsai-Shien Chen, Aliaksandr Siarohin, Willi Menapace, Ekaterina Deyneka, Hsiang-wei Chao, Byung Eun Jeon, Yuwei Fang, Hsin-Ying Lee, Jian Ren, Ming-Hsuan Yang, and Sergey Tulyakov. Panda-70m: Captioning 70m videos with multiple cross-modality teachers. In *CVPR*, 2024. 2
- [11] Zhenghao Chen, Guo Lu, Zhihao Hu, Shan Liu, Wei Jiang, and Dong Xu. Lsvc: A learning-based stereo video compression framework. In *Proceedings of the IEEE/CVF Conference on Computer Vision and Pattern Recognition*, pages 6073–6082, 2022. 9
- [12] Zhenghao Chen, Lucas Relic, Roberto Azevedo, Yang Zhang, Markus Gross, Dong Xu, Luping Zhou, and Christopher Schroers. Neural video compression with spatio-temporal cross-covariance transformers. In *Proceedings of the 31st ACM International Conference on Multimedia*, pages 8543–8551, 2023. 9
- [13] Zhenghao Chen, Luping Zhou, Zhihao Hu, and Dong Xu. Group-aware parameter-efficient updating for content-adaptive neural video compression. In *Proceedings of the 32nd ACM International Conference on Multimedia*, pages 11022–11031, 2024. 1
- [14] Patrick Esser, Robin Rombach, and Bjorn Ommer. Taming transformers for high-resolution image synthesis. In *CVPR*, pages 12873–12883, 2021. 8
- [15] Gongfan Fang, Xinyin Ma, Mingli Song, Michael Bi Mi, and Xinchao Wang. Depgraph: Towards any structural pruning. In *CVPR*, 2023. 1, 2, 3, 6, 12
- [16] Gongfan Fang, Xinyin Ma, and Xinchao Wang. Structural pruning for diffusion models. In *NeurIPS*, 2023. 3
- [17] Songwei Ge, Aniruddha Mahapatra, Gaurav Parmar, Jun-Yan Zhu, and Jia-Bin Huang. On the content bias in fréchet video distance. In *CVPR*, pages 7277–7288, 2024. 6
- [18] Ian Goodfellow, Jean Pouget-Abadie, Mehdi Mirza, Bing Xu, David Warde-Farley, Sherjil Ozair, Aaron Courville, and Yoshua Bengio. Generative adversarial networks. *Communications of the ACM*, 63(11):139–144, 2020. 2
- [19] Yuwei Guo, Ceyuan Yang, Anyi Rao, Zhengyang Liang, Yao-hui Wang, Yu Qiao, Maneesh Agrawala, Dahua Lin, and Bo Dai. Animatediff: Animate your personalized text-to-image diffusion models without specific tuning. In *ICLR*, 2024. 2
- [20] Song Han, Jeff Pool, John Tran, and William J Dally. Learning both weights and connections for efficient neural network. In *NeurIPS*, 2015. 1, 2
- [21] Geoffrey Hinton, Oriol Vinyals, and Jeff Dean. Distilling the knowledge in a neural network. In *NIPS Workshop*, 2014. 1, 2
- [22] Jonathan Ho and Tim Salimans. Classifier-free diffusion guidance. In *NeurIPS 2021 Workshop on Deep Generative Models and Downstream Applications*, 2021. 3
- [23] Jonathan Ho, Tim Salimans, Alexey Gritsenko, William Chan, Mohammad Norouzi, and David J Fleet. Video diffusion models. In *NeurIPS*, pages 8633–8646, 2022. 2
- [24] Torsten Hoeffler, Dan Alistarh, Tal Ben-Nun, Nikoli Dryden, and Alexandra Peste. Sparsity in deep learning: Pruning and growth for efficient inference and training in neural networks. *JMLR*, 22(241):1–124, 2021. 1
- [25] Ziqi Huang, Yanan He, Jiashuo Yu, Fan Zhang, Chenyang Si, Yuming Jiang, Yuanhan Zhang, Tianxing Wu, Qingyang Jin, Nattapol Chanpaisit, Yaohui Wang, Xinyuan Chen, Limin

- Wang, Dahua Lin, Yu Qiao, and Ziwei Liu. Vbench: Comprehensive benchmark suite for video generative models. In *CVPR*, 2024. 6
- [26] Tero Karras, Miika Aittala, Timo Aila, and Samuli Laine. Elucidating the design space of diffusion-based generative models. pages 26565–26577, 2022. 3
- [27] Tero Karras, Miika Aittala, Jaakko Lehtinen, Janne Hellsten, Timo Aila, and Samuli Laine. Analyzing and improving the training dynamics of diffusion models. In *CVPR*, pages 24174–24184, 2024. 3
- [28] Levon Khachatryan, Andranik Movsisyan, Vahram Tadevosyan, Roberto Henschel, Zhangyang Wang, Shant Navasardyan, and Humphrey Shi. Text2video-zero: Text-to-image diffusion models are zero-shot video generators. In *CVPR*, pages 15954–15964, 2023. 2
- [29] Bo-Kyeong Kim, Hyoung-Kyu Song, Thibault Castells, and Shinkook Choi. Bk-sdm: A lightweight, fast, and cheap version of stable diffusion. In *ECCV*, 2024. 1, 2, 3, 4
- [30] Diederik P Kingma. Auto-encoding variational bayes. *arXiv preprint arXiv:1312.6114*, 2013. 2
- [31] PKU-Yuan Lab and Tuzhan AI etc. Open-sora-plan, 2024. 2
- [32] Luma Labs. Dream machine. <https://lumalabs.ai/dream-machine>, 2024. 1
- [33] Hao Li, Asim Kadav, Igor Durdanovic, Hanan Samet, and Hans Peter Graf. Pruning filters for efficient convnets. In *ICLR*, 2017. 1, 2, 6
- [34] Jiachen Li, Qian Long, Jian Zheng, Xiaofeng Gao, Robinson Piramuthu, Wenhu Chen, and William Yang Wang. T2v-turbo-v2: Enhancing video generation model post-training through data, reward, and conditional guidance design. *arXiv preprint arXiv:2410.05677*, 2024. 2, 6, 7, 13
- [35] Yanyu Li, Huan Wang, Qing Jin, Ju Hu, Pavlo Chemerys, Yun Fu, Yanzhi Wang, Sergey Tulyakov, and Jian Ren. Snapfusion: Text-to-image diffusion model on mobile devices within two seconds. In *NeurIPS*, 2023. 1, 2, 3, 12
- [36] Pengyang Ling, Jiazi Bu, Pan Zhang, Xiaoyi Dong, Yuhang Zang, Tong Wu, Huaian Chen, Jiaqi Wang, and Yi Jin. Motionclone: Training-free motion cloning for controllable video generation. *arXiv preprint arXiv:2406.05338*, 2024. 13
- [37] Simian Luo, Yiqin Tan, Longbo Huang, Jian Li, and Hang Zhao. Latent consistency models: Synthesizing high-resolution images with few-step inference. *arXiv preprint arXiv:2310.04378*, 2023. 3
- [38] Xiaofeng Mao, Zhengkai Jiang, Fu-Yun Wang, Wenbing Zhu, Jiangning Zhang, Hao Chen, Mingmin Chi, and Yabiao Wang. Osv: One step is enough for high-quality image to video generation. *arXiv preprint arXiv:2409.11367*, 2024. 1
- [39] Chenlin Meng, Ruiqi Gao, Diederik P Kingma, Stefano Ermon, Jonathan Ho, and Tim Salimans. On distillation of guided diffusion models. In *CVPR*, 2023. 2
- [40] Pavlo Molchanov, Stephen Tyree, Tero Karras, Timo Aila, and Jan Kautz. Pruning convolutional neural networks for resource efficient inference. In *ICLR*, 2017. 3
- [41] Michael C Mozer and Paul Smolensky. Skeletonization: A technique for trimming the fat from a network via relevance assessment. In *NeurIPS*, 1988. 3
- [42] Kepan Nan, Rui Xie, Penghao Zhou, Tiehan Fan, Zhenheng Yang, Zhijie Chen, Xiang Li, Jian Yang, and Ying Tai. Openvid-1m: A large-scale high-quality dataset for text-to-video generation. *arXiv preprint arXiv:2407.02371*, 2024. 5, 12
- [43] OpenAI. Sora. <https://openai.com/index/video-generation-models-as-world-simulators/>, 2024. 2
- [44] William Peebles and Saining Xie. Scalable diffusion models with transformers. 2023. 2
- [45] Russell Reed. Pruning algorithms - a survey. *IEEE transactions on Neural Networks*, 4(5):740–747, 1993. 1
- [46] Tim Salimans and Jonathan Ho. Progressive distillation for fast sampling of diffusion models. In *ICLR*, 2022. 2
- [47] Axel Sauer, Frederic Boesel, Tim Dockhorn, Andreas Blattmann, Patrick Esser, and Robin Rombach. Fast high-resolution image synthesis with latent adversarial diffusion distillation. *arXiv preprint arXiv:2403.12015*, 2024. 13
- [48] Ivan Skorokhodov, Sergey Tulyakov, and Mohamed Elhoseiny. Stylegan-v: A continuous video generator with the price, image quality and perks of stylegan2. In *CVPR*, pages 3626–3636, 2022. 6, 12
- [49] Jiaming Song, Chenlin Meng, and Stefano Ermon. Denoising diffusion implicit models. 2021. 2
- [50] Yang Song and Prafulla Dhariwal. Improved techniques for training consistency models. In *ICLR*, 2024. 1, 3
- [51] Yang Song, Jascha Sohl-Dickstein, Diederik P Kingma, Abhishek Kumar, Stefano Ermon, and Ben Poole. Score-based generative modeling through stochastic differential equations. In *ICLR*, 2021. 3
- [52] Yang Song, Prafulla Dhariwal, Mark Chen, and Ilya Sutskever. Consistency models. In *ICML*, pages 127–144, 2023. 1, 3
- [53] Zhiyu Tan, Xiaomeng Yang, Luozheng Qin, and Hao Li. Vidgen-1m: A large-scale dataset for text-to-video generation. *arXiv preprint arXiv:2408.02629*, 2024. 5
- [54] Fu-Yun Wang, Zhaoyang Huang, Xiaoyu Shi, Weikang Bian, Guanglu Song, Yu Liu, and Hongsheng Li. Animate1cm: Computation-efficient personalized style video generation without personalized video data. 2024. 1, 6
- [55] Huan Wang, Can Qin, Yulun Zhang, and Yun Fu. Neural pruning via growing regularization. In *ICLR*, 2021. 1, 2
- [56] Zhendong Wang, Huangjie Zheng, Pengcheng He, Weizhu Chen, and Mingyuan Zhou. Diffusion-gan: Training gans with diffusion. In *ICLR*, 2023. 5
- [57] Yanwu Xu, Yang Zhao, Zhisheng Xiao, and Tingbo Hou. Ufo-gen: You forward once large scale text-to-image generation via diffusion gans. In *CVPR*, 2024. 3
- [58] Zhuoyi Yang, Jiayan Teng, Wendi Zheng, Ming Ding, Shiyu Huang, Jiazhen Xu, Yuanming Yang, Wenyi Hong, Xiaohan Zhang, Guanyu Feng, et al. Cogvideox: Text-to-video diffusion models with an expert transformer. *arXiv preprint arXiv:2408.06072*, 2024. 2
- [59] Yuanhao Zhai, Kevin Lin, Zhengyuan Yang, Linjie Li, Jianfeng Wang, Chung-Ching Lin, David Doermann, Junsong Yuan, and Lijuan Wang. Motion consistency model: Accelerating video diffusion with disentangled motion-appearance distillation. In *NeurIPS*. 1

- [60] Yabo Zhang, Yuxiang Wei, Dongsheng Jiang, XIAOPENG ZHANG, Wangmeng Zuo, and Qi Tian. Controlvideo: Training-free controllable text-to-video generation. In *ICLR*, 2024. [2](#)
- [61] Zhixing Zhang, Yanyu Li, Yushu Wu, Yanwu Xu, Anil Kag, Ivan Skorokhodov, Willi Menapace, Aliaksandr Siarohin, Junli Cao, Dimitris Metaxas, et al. Sf-v: Single forward video generation model. In *NeurIPS*, 2024. [1](#), [2](#), [3](#), [6](#), [12](#)
- [62] Yang Zhao, Yanwu Xu, Zhisheng Xiao, and Tingbo Hou. Mobicdiffusion: Subsecond text-to-image generation on mobile devices. *arXiv preprint arXiv:2311.16567*, 2023. [3](#)
- [63] Zangwei Zheng, Xiangyu Peng, Tianji Yang, Chenhui Shen, Shenggui Li, Hongxin Liu, Yukun Zhou, Tianyi Li, and Yang You. Open-sora: Democratizing efficient video production for all, 2024. [2](#), [4](#)

The appendix part of this work consists of two parts which are:

- This **document** providing details about App. A., the compression of the VAE decoder of SF-V, App. B, the compressed U-Net, App. C, I2V and T2V baselines.
- Additional **videos**. We also provide supplementary videos demonstrating the qualitative results of the videos generated by VDMini-I2V and VDMini-T2V.

## A. Compression of the VAE Decoder of SF-V

The VAE decoder in the I2V method SF-V incurs significant inference time. Therefore, we follow [35] to apply both layer pruning and channel pruning techniques [15] to compress the VAE decoder, which will further reduce the inference time for SF-V. Initially, we present the block-wise architecture of the VAE decoder in Fig. A1 and the block-wise inference time and the number of parameters in Fig. A2. Our observations indicate that the latter layers of the VAE decoder, which handle higher resolution features, consume most of the inference time. Specifically, we remove layers in the “MidBlock” and “UpBlock.3”, as these layers significantly contribute to inference time and model weight. Subsequently, we utilize Torch-Pruning [15] for channel pruning to further accelerate the model. This results in a compressed VAE decoder with a 70% reduction in inference time and a 30% reduction in the number of parameters. By fine-tuning the compressed VAE decoder on the OpenVid-1M dataset [42] using reconstruction loss, perceptual loss, and adversarial loss, we achieve performance comparable to the original VAE decoder.

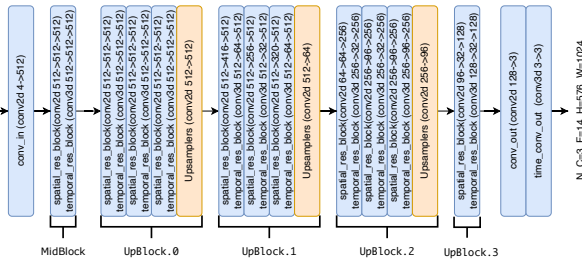


Figure A1. Network architecture of the compressed VAE decoder. First, we remove the layers in MidBlock and UpBlock.3, then perform channel pruning to speed up inference time.

## B. Details about the Compressed U-Net

As discussed in Sec. 3.2, most I2V and T2V models share nearly identical architectures in their diffusion model backbone (*i.e.*, U-Net), we hold an assumption that specific blocks within these U-Nets perform similar roles across both tasks. Hence, in this work, we focus on providing an in-depth analysis of the I2V model SF-V and extend our observations to the T2V model T2V-Turbo-v2.

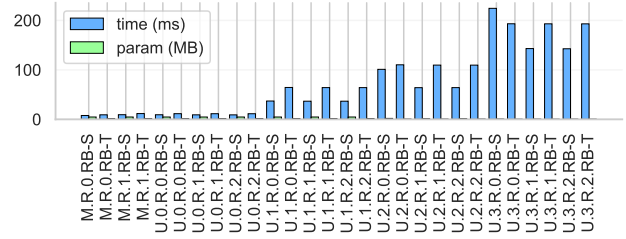


Figure A2. Time and Parameters of the blocks in the VAE decoder.

Specifically, we study the **importance score** and the **computational complexity** for U-Net of SF-V. First, we present the detailed block-wise importance scores by replacing the blocks with identity mapping or a single convolutional layer, as shown in Fig. A3. A higher FVD score indicates a more important block. The FVD score calculation follows the evaluation protocol introduced in StyleGAN-V [48]. For fast evaluation, we sample 1200 videos from the UCF101 dataset as the ground-truth videos and calculate the FVD score between the generated and ground-truth videos. As illustrated in Fig. A3, we use a specific notation to denote the blocks in the U-Net. For example, the module named “D.1.R.0.RB-S” indicates: “D” for DownBlock, “1” for the first subblock, “R” for ResBlock type, “0” for the layer index of the ResBlock, and “RB-S” for SpatialResBlock consisting of 2D ResNet blocks. The results show that the SpatialResBlock in the DownBlocks is more important than other sub-blocks, and in the UpBlocks, the SpatialAttentionBlock is more important. Second, we present the computational complexity study including the inference time and the number of parameters for each block in the U-Net of SF-V, as shown in Fig. A4. The inference time measurement is conducted on a single NVIDIA A100 GPU.

According to the above observations, we propose the following pruning strategy for VDMini. 1) completely remove the “Down-3”, “Mid”, and “Up-0” blocks in VDMini, and 2) reduce the number of blocks in “Down-0”, “Down-1”, “Up-2”, and “Up-3” by one compared to the original U-Net.

As explained previously, we directly apply our observations regarding U-Net compression from the I2V model to the T2V model. Consequently, as shown in Tab. A1, the pruned models VDMini-T2V and VDMini-I2V share an almost identical architecture, with only minor differences in the structure of the “ResBlock.” Specifically, in VDMini-T2V, the ResBlock is a 2D ResNet block, while in VDMini-I2V, it consists of both a 2D ResBlock and a 3D ResBlock.

## C. Implementation of I2V and T2V Baselines

Here, we introduce the implementation details of our I2V and T2V baseline methods SF-V and T2V-Turbo-v2.

**SF-V**: [61] is a one-step I2V model fine-tuned from Stable Video Diffusion (SVD) [3] on a 1M internal video dataset.

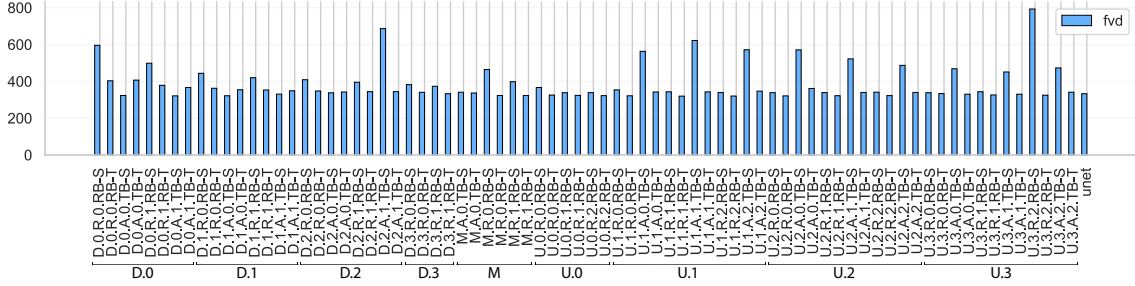


Figure A3. Block-wise FVD score by removing or replacing the blocks in the U-Net.

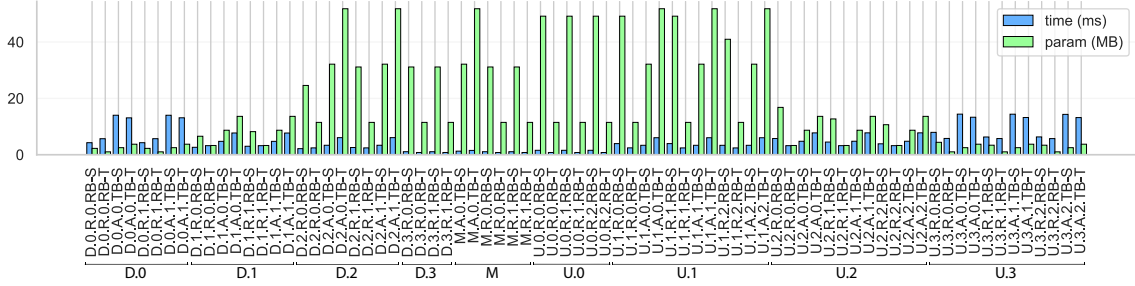


Figure A4. Block-wise inference time and parameter count in the U-Net.

Stage	Resolution	Type	Config	UNet Model	
				Origin	Ours
Down-0	$T \times \frac{H}{8} \times \frac{W}{8}$	ResBlock	Dimension # Blocks	320 2	320 1
		TransformerBlock	Dimension # Blocks	320 2	320 1
Down-1	$T \times \frac{H}{16} \times \frac{W}{16}$	ResBlock	Dimension # Blocks	640 2	640 1
		TransformerBlock	Dimension # Blocks	640 2	640 1
Down-2	$T \times \frac{H}{32} \times \frac{W}{32}$	ResBlock	Dimension # Blocks	1280 2	1280 2
		TransformerBlock	Dimension # Blocks	1280 2	1280 2
Down-3	$T \times \frac{H}{64} \times \frac{W}{64}$	ResBlock	Dimension # Blocks	1280 2	1280 0
		TransformerBlock	Dimension # Blocks	1280 1	1280 0
Mid	$T \times \frac{H}{64} \times \frac{W}{64}$	ResBlock	Dimension # Blocks	1280 2	1280 0
		TransformerBlock	Dimension # Blocks	1280 1	1280 0
Up-0	$T \times \frac{H}{64} \times \frac{W}{64}$	ResBlock	Dimension # Blocks	1280 3	1280 0
		TransformerBlock	Dimension # Blocks	1280 3	1280 3
Up-1	$T \times \frac{H}{32} \times \frac{W}{32}$	ResBlock	Dimension # Blocks	1280 3	1280 3
		TransformerBlock	Dimension # Blocks	1280 3	1280 3
Up-2	$T \times \frac{H}{16} \times \frac{W}{16}$	ResBlock	Dimension # Blocks	640 3	640 2
		TransformerBlock	Dimension # Blocks	640 3	640 2
Up-3	$T \times \frac{H}{8} \times \frac{W}{8}$	ResBlock	Dimension # Blocks	320 3	320 2
		TransformerBlock	Dimension # Blocks	320 3	320 2

Table A1. The detailed architecture of the compressed U-Net used in VDMini.

SF-V follows LADD [47] to fine-tune the pre-trained SVD with adversarial loss, with the discriminator initialized from the pre-trained SVD. Since the code and model of SVD are not publicly available, we re-implemented the SF-V model

using the OpenVid-1M dataset, a high-quality video dataset with dense captions. We adhered to the original SF-V training settings, with a batch size of 32 and a gradient accumulation step of 4. The learning rates for the U-Net and the heads of the discriminator were set to  $1e-5$  and  $1e-4$ , respectively. After 50K training steps, we achieved an FVD score of 166.26, comparable to the original SF-V model.

**T2V-Turbo-v2** [34] is a T2V model, which is distilled from VideoCrafter2 [9] and follows a consistency distillation scheme. The initial version of T2V-Turbo (*i.e.* T2V-Turbo-v1) adopts mixed reward models to enhance the generation quality and prompt consistency, and T2V-Turbo-v2 further employs MotionClone [36] to enhance the motion dynamics in the few-step sampling, and the resulting model achieves the first rank in the VBench leaderboard. The U-Net architecture of T2V-Turbo-v2 is similar to SVD.